"Quasi-monochromatic cerium flash angiography," *SPIE*, **5580**, 146-152, 2005.
13. E. Sato, E. Tanaka, H. Mori, T. Kawai, T. Inoue, A. Ogawa, S. Sato, K. Takayama and H. Ido, "High-speed K-edge angiography achieved with tantalum K-series characteristic x rays," *SPIE*, **5745**, 810-817, 2005.
14. H. Obara, E. Sato, E. Tanaka, H. Mori, T. Kawai, S. Sato, H. Ojima, K. Takayama and H. Ido, "Superposition of x-ray spectra using a double-target plasma tube," *SPIE*, **5580**, 824-831, 2005.
15. E. Sato, K. Sato and Y. Tamakawa, "Film-less computed radiography system for high-speed imaging," *Ann. Rep. Iwate Med. Univ. Sch. Lib. Arts and Sci.*, **35**, 13-23, 2000.
*obara@rad.cms.tohoku.ac.jp; phone +81-22-717-7941; fax +81-22-717-7944

Superposition of x-ray spectra using double-target plasma triode

Haruo Obara*[a], Eiichi Sato[b], Etsuro Tanaka[c], Hidezo Mori[d], Toshiaki Kawai[e], Shigehiro Sato[f], Hidenori Ojima[g], Kazuyoshi Takayama[g] and Hideaki Ido[h]

[a] Department of Radiological Technology, College of Medical Science, Tohoku University, 1-1 Seiryocho, Sendai 980-0872, Japan
[b] Department of Physics, Iwate Medical University, 3-16-1 Honchodori, Morioka 020-0015, Japan
[c] Department of Nutritional Science, Faculty of Applied Bio-science, Tokyo University of Agriculture, 1-1-1 Sakuragaoka, Setagaya-ku 156-8502, Japan
[d] Department of Cardiac Physiology, National Cardiovascular Center Research Institute, 5-7-1 Fujishirodai, Suita, Osaka 565-8565, Japan
[e] Electron Tube Division #2, Hamamatsu Photonics K. K., 314-5 Shimokanzo, Toyooka Village, Iwata-gun 438-0193, Japan
[f] Department of Microbiology, School of Medicine, Iwate Medical University, 19-1 Uchimaru, Morioka 020-8505, Japan
[g] Shock Wave Research Center, Institute of Fluid Science, Tohoku University, 2-1-1 Katahira, Sendai 980-8577, Japan
[h] Department of Applied Physics and Informatics, Faculty of Engineering, Tohoku Gakuin University, 1-13-1 Chuo, Tagajo 985-8537, Japan

ABSTRACT

In the plasma flash x-ray generator, a 200 nF condenser is charged up to 50 kV by a power supply, and flash x rays are produced by the discharging. The x-ray tube is a demountable triode with a double target consisting of a copper and a molybdenum rods, and the turbomolecular pump evacuates air from the tube with a pressure of approximately 1 mPa. Target evaporation leads to the formation of weakly ionized linear plasma, consisting of metal ions and electrons, around the fine target, and intense characteristic x rays are produced. At a charging voltage of 50 kV, the maximum tube voltage was almost equal to the charging voltage of the main condenser, and the peak current was about 11 kA. When the charging voltage was increased, the linear plasma formed, and the molybdenum K-series characteristic x-ray intensities increased substantially. Although the intensities of copper Kα lines increased with increases in the charging voltage, hardly any clean Kβ lines were detected. The x-ray pulse widths were approximately 1.2 μs, and the time-integrated x-ray intensity was approximately 30 μC/kg at 1.0 m from the x-ray source with a charging voltage of 50 kV.

Keywords: flash x-ray, plasma x-ray, weakly ionized linear plasma, characteristic x rays, x-ray superposition

1. INTRODUCTION

Monochromatic x-ray computed tomography at two different energies has provided information about the electron density of human tissue.[1] In addition, a compact pulsed tunable monochromatic x-ray source has been designed, developed, and tested.[2] From the source, cone x-ray beams from 10 to 50 keV with pulse widths of 8 ps have been produced, and these beams are useful for biomedical imaging and protein crystallography.

Most flash x-ray generators utilize surge Marx generators[3,4] in conjunction with cold-cathode diodes and produce extremely short x-ray pulses with durations of less than 1 μs. In the surge generator, the output voltage is equal to the value of the condenser charging voltage multiplied by the stage number. Because the high-voltage durability substantially increased under the pulsed operation, the maximum photon energy of flash x rays has been increased to 1 MeV or beyond so as to perform military applications.

To perform biomedical radiography, we have developed several different soft flash x-ray generators[5-10] corresponding to specific radiographic objectives, and a major goal in our research is the development of an intense and clean

26th International Congress on High-Speed Photography and Photonics, edited by D. L. Paisley, S. Kleinfelder, D. R. Snyder, B. J. Thompson, Proc. of SPIE Vol. 5580 (SPIE, Bellingham, WA, 2005) · 0277-786X/05/$15 · doi: 10.1117/12.581235

monochromatic x-ray generator that can impact applications with biomedical radiography with photon energies of approximately 10 keV or beyond. In view of this situation, we confirmed irradiation of intense K-series characteristic x rays from the plasma axial direction by forming weakly ionized linear plasma.[11-15] On the other hand, we are very interested in the superposition of characteristic x rays in order to perform wide latitude radiography or energy subtraction radiography.
In this paper, we describe a plasma flash x-ray generator utilizing a double-target radiation tube, used to perform a preliminary experiment for the superposition of characteristic x rays

2. GENERATOR

2.1 High-voltage circuit

Figure 1 shows a block diagram of a high-intensity plasma flash x-ray generator. The generator consists of the following essential components: a high-voltage power supply, a high-voltage condenser with a capacity of approximately 200 nF, a turbomolecular pump, a krytron pulse generator as a trigger device, and a flash x-ray tube. In this generator, a low-impedance transmission line is employed in order to increase maximum tube current (Fig. 2). The high-voltage main condenser is charged up to 50 kV by the power supply, and electric charges in the condenser are discharged to the tube after triggering the cathode electrode with the trigger device. The plasma flash x rays are then produced.

2.2 X-ray tube

The x-ray tube is a demountable cold-cathode triode that is connected to the turbomolecular pump with a pressure of approximately 1 mPa (Fig. 3). This tube consists of the following major parts: a pipe-shaped graphite cathode with a bore diameter of 10.0 mm, a trigger electrode made from copper wire, a brass focusing electrode, a stainless-steel vacuum chamber, a nylon insulator, a polyethylene terephthalate (Mylar) x-ray window 0.25 mm in thickness, and a double-rod target. The target is composed of a copper rod and a molybdenum rod each 2.0 mm in diameter, and the plasma length is primarily determined by the distance between the target tip and the graphite ring. The distance between the target and cathode electrodes is approximately 20 mm, and the trigger electrode is set in the cathode electrode. As electron beams from the cathode electrode are roughly converged to the target by the focusing electrode, evaporation leads to the formation of weakly ionized linear plasma, consisting of metal ions and electrons, around the fine target.

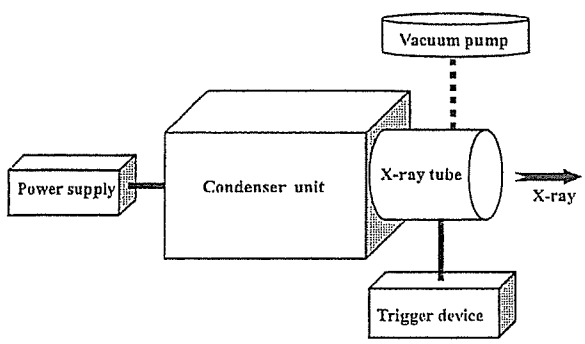

Figure 1: Block diagram of high-intensity plasma flash x-ray generator.

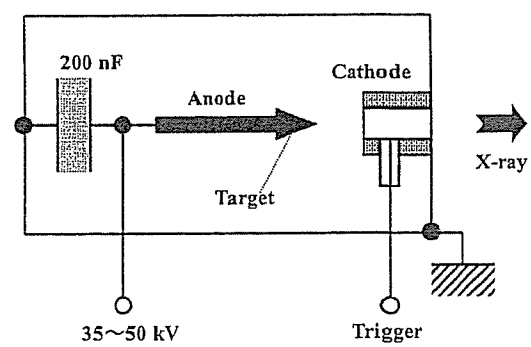

Figure 2: Circuit diagram of flash x-ray generator.

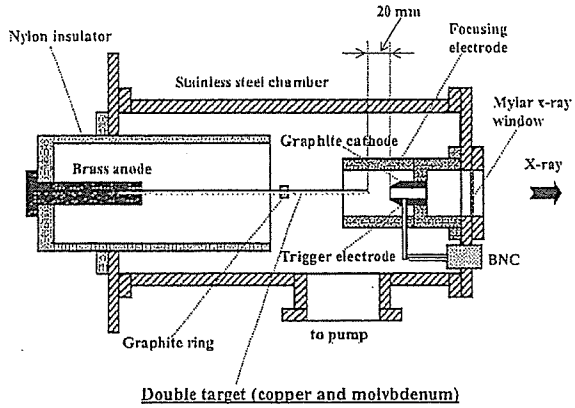

Figure 3: Schematic drawing of flash x-ray tube with double target.

3. CHARACTERISTICS

3.1 Tube voltage and current

Tube voltage and current were measured by a high-voltage divider with an input impedance of 1 GΩ and a current transformer, respectively. Figure 4 shows the time relation between the tube voltage and current. At the indicated charging voltages, they roughly displayed damped oscillations. When the charging voltage was increased, both the maximum tube voltage and current increased. At a charging voltage of 50 kV, the maximum tube voltage was almost equal to the charging voltage of the main condenser, and the maximum tube current was approximately 11 kA.

3.2 X-ray output

X-ray output pulse was detected using a combination of a plastic scintillator and a photomultiplier (Fig. 5). The x-ray pulse height substantially increased with corresponding increases in the charging voltage. The x-ray pulse widths were about 1.2 μs, and the time-integrated x-ray intensity measured by a thermoluminescence dosimeter (Kyokko TLD Reader 1500 with MSO-S elements without energy compensation) had a value of approximately 30 μC/kg at 1.0 m from the x-ray source with a charging voltage of 50 kV.

3.3 X-ray source

In order to roughly observe images of the plasma x-ray source in the detector plane, we employed a 100-μm-diameter pinhole camera and an x-ray film (Polaroid XR-7) (Fig. 6). At a charging voltage of 35 kV, we observed two spots of the double target. When the charging voltage was increased, the plasma x-ray source grew, and both spot dimension and intensity increased. Because the x-ray intensity is the highest at the center of the two targets, both the dimension and intensity decreased according to both increases in the thickness of a filter for absorbing x rays and decreases in the pinhole diameter.

3.4 X-ray spectra

X-ray spectra from the plasma source were measured by a transmission-type spectrometer with a lithium fluoride curved crystal 0.5 mm in thickness. The spectra were taken by a computed radiography (CR) system[16] with a wide dynamic range, and relative x-ray intensity was calculated from Dicom digital data.

Figure 7 shows measured spectra near molybdenum K-series characteristic x rays. We observed sharp lines of K-series characteristic x rays of molybdenum. However bremsstrahlung rays were only detected slightly. The molybdenum characteristic x-ray intensity substantially increased with corresponding increases in the charging voltage. In the measurement of copper spectra (Fig. 8), although fairly clean Kα lines were observed, any sharp Kβ lines were hardly detected. In addition, we found lines of $0.5E_{\alpha}$, but $0.5E_{\beta}$ lines were not detected. Here, E_{α} and E_{β} are the average photon energies of molybdenum Kα and Kβ lines, respectively.

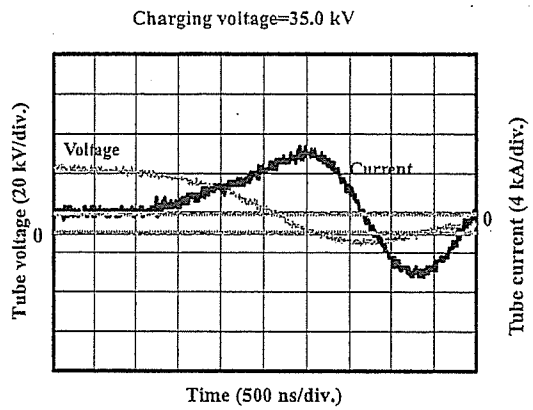

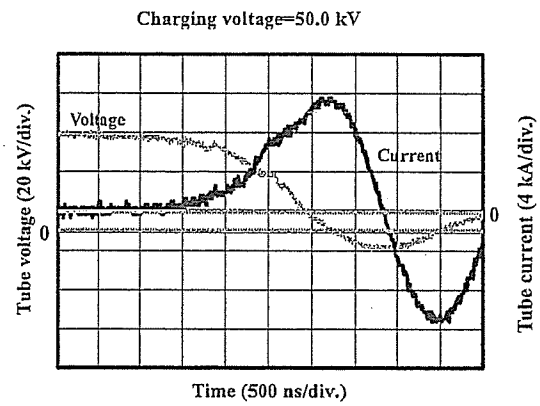

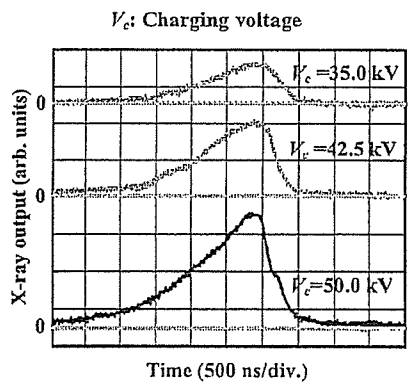

Figure 5: X-ray outputs at indicated conditions.

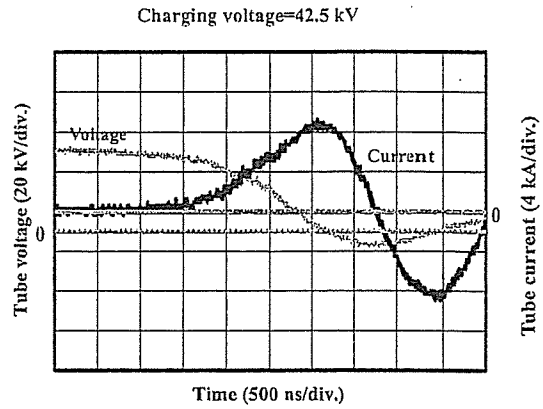

Figure 4: Tube voltages and currents with changing charging voltage.

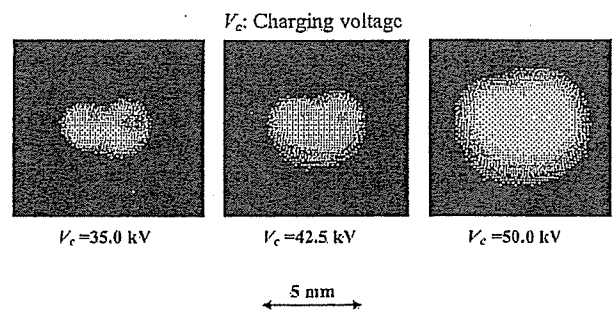

Figure 6: Images of plasma x-ray source of double target.

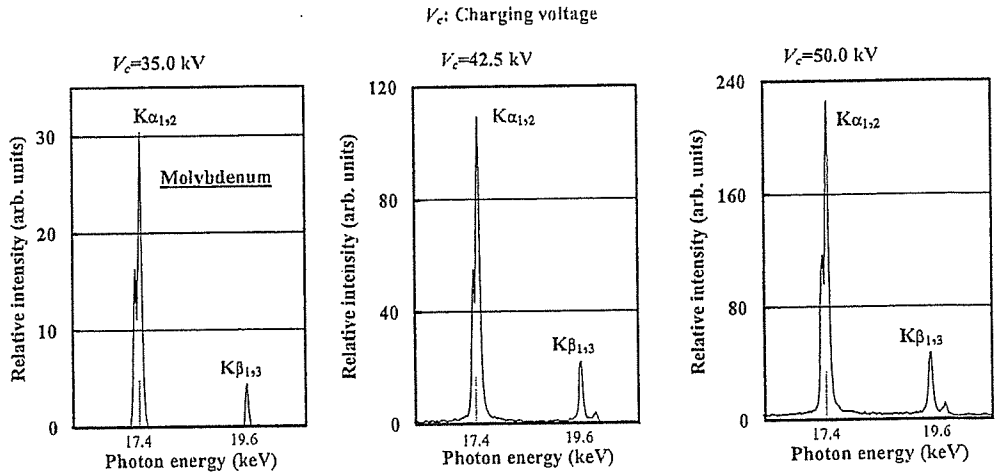

Figure 7: X-ray spectra near molybdenum K-series characteristic x rays.

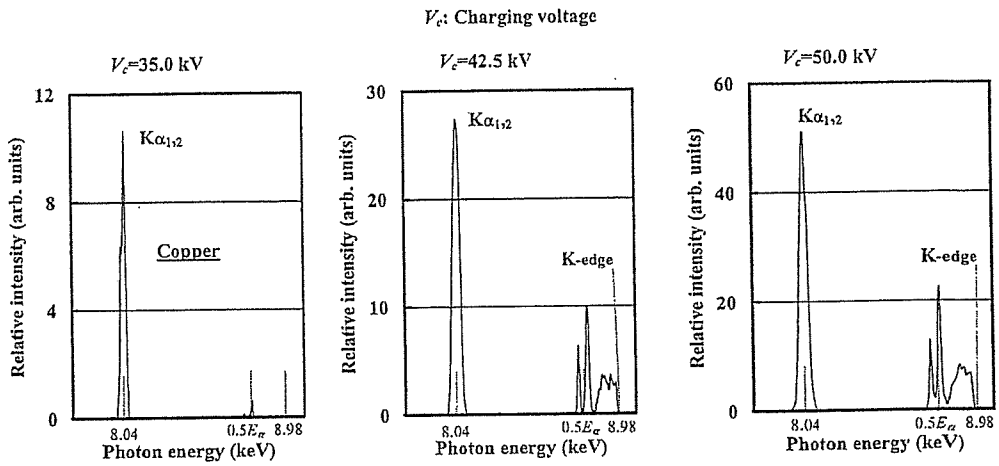

Figure 8: X-ray spectra near copper K-series characteristic x rays.

4. RADIOGRAPHY

The plasma radiography was performed by the CR system (Konica Regius 150) without using a filter, and the distance between the x-ray source and imaging plate was 1.2 m.

Figure 9 shows radiograms of tungsten wires coiled around a pipe made of polymethyl methacrylate with a charging voltage of 45 kV. Although the image contrast increased with increases in the wire diameter, a 50-μm-diameter wire could be observed. Next, the image of water falling into a polypropylene beaker from an glass test tube is shown in Fig. 10. This image was taken with a charging voltage of 50 kV, and an iodine-based contrast medium was added a little. Because the x-ray duration was about 1 μs, the stop-motion image of water was obtained. Figure 11 shows an angiogram of the external ear of a rabbit with a charging voltage (V_c) of 45 kV. In angiography, iodine-based microspheres of 15 μm in diameter were used, and fine blood vessels of about 100 μm are clearly visible. Figures 12 and 13 show angiograms of a rabbit heart (V_c=45 kV) and a thigh (V_c=50 kV), respectively, and fine blood vessels were visible.

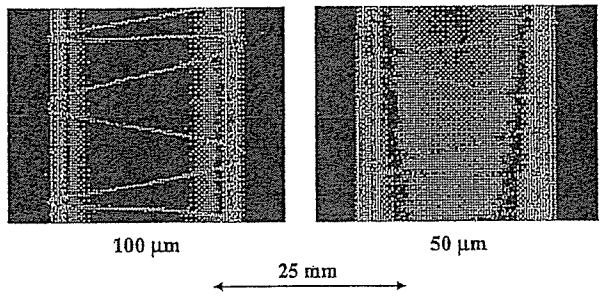

Figure 9: Radiograms of tungsten wires coiled around pipe made of polymethyl methacrylate.

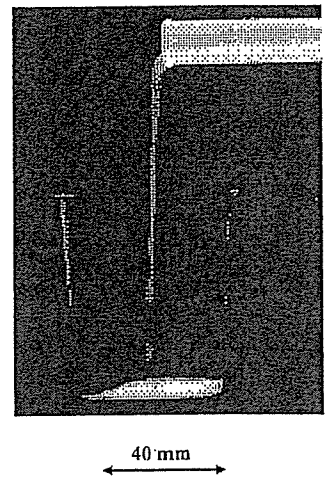

Figure 10: Radiogram of water from glass test tube.

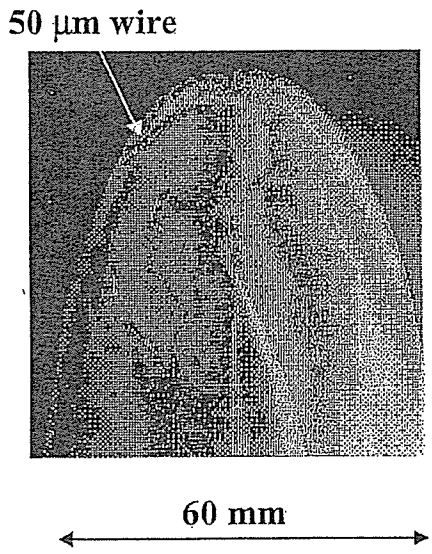

Figure 11: Angiogram of external ear.

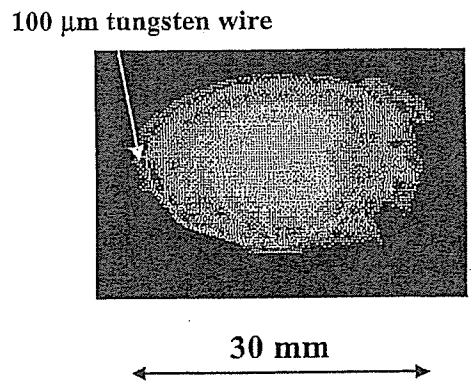

Figure 12: Angiogram of rabbit heart.

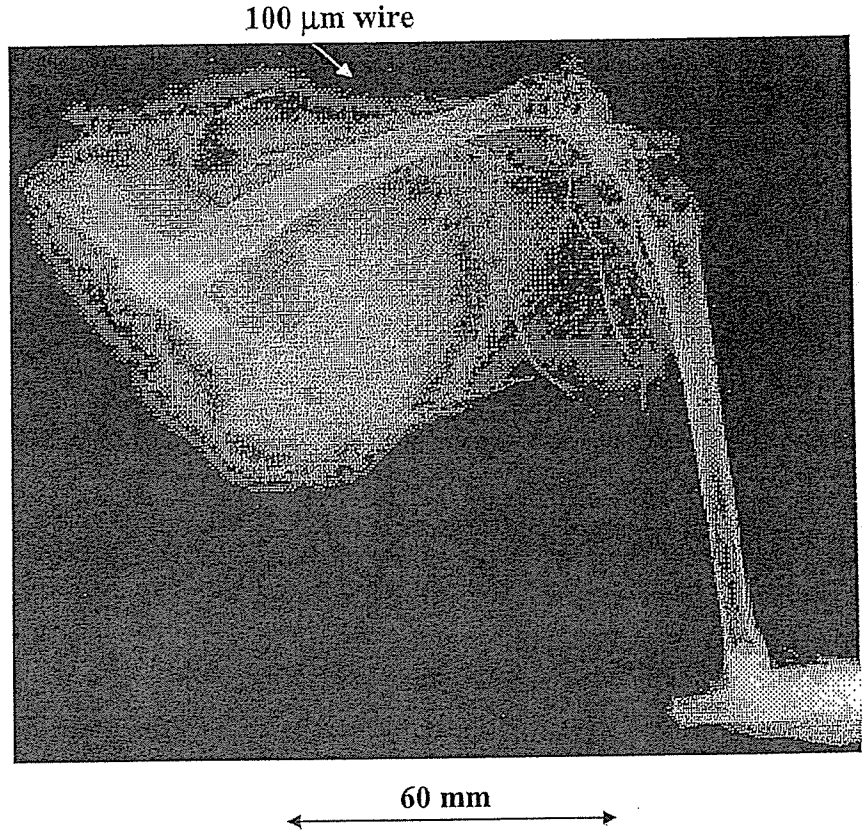

Figure 13: Angiogram of rabbit thigh.

5. DISCUSSION

Regarding the spectrum measurement, although we obtained intense and sharp molybdenum K-series lines, we could not observe copper Kβ lines. In addition, we observed $0.5E_{\alpha}$ lines and the copper K-absorption edge. If we assume that the $0.5E_{\alpha}$ lines are molybdenum Kα lines detected by the high order diffraction, the molybdenum Kβ lines, the copper Kβ lines, and the bremsstrahlung rays should be observed.
In this research, we obtained sufficient characteristic x-ray intensity per pulse for CR radiography without using a monochromatic filter, and the generator produced number of characteristic photons was approximately 4×10^{8} photons/cm^2 at 1.0 m per pulse. In addition, since the photon energy of characteristic x rays can be controlled by changing target elements, various quasi-monochromatic high-speed radiographies, such as flash energy subtraction radiography using a metal filter and wide latitude radiography, will be possible.

ACKNOWLEDGMENT

This work was supported by Grants-in-Aid for Scientific Research (13470154, 13877114, 16591181and 16591222) and Advanced Medical Scientific Research from MECSST, Health and Labor Sciences Research Grants(RAMT-nano-001, RHGTEFB-genome-005 and RHGTEFB-saisei-003), Grants from Keiryo Research Foundation, The Promotion and Mutual Aid Corporation for Private Schools of Japan, Japan Science and Technology Agency (JST), and New Energy and Industrial Technology Development Organization (NEDO, Industrial Technology Research Grant Program in '03).

REFERENCES

1. M. Torikoshi, T. Tsunoo, M. Sasaki, M. Endo, Y. Noda, T. Kohno, K. Hyodo, K. Uesugi and N. Yagi: "Electron density measurement with dual-energy x-ray CT using synchrotron radiation," *Phys. Med. Biol.*, **48**, 673-685, 2003.
2. F. E. Carroll, M. H. Mendenhall, R. H. Traeger, C. Brau and J. W. Waters, "Pulsed tunable monochromatic x-ray beams from a compact source: New opportunities," *Am. J. Roentgenol.*, **181**, 1197-1202, 2003.
3. A. Mattsson, "Some characteristics of a 600 kV flash x-ray tube," *Physica Scripta*, **5**, 99-102, 1972.
4. R. Germer, "X-ray flash techniques," *J. Phys. E: Sci. Instrum.*, **12**, 336-350, 1979.
5. E. Sato, H. Isobe and F. Hoshino, "High intensity flash x-ray apparatus for biomedical radiography," *Rev. Sci. Instrum.*, **57**, 1399-1408, 1986.
6. E. Sato, S. Kimura, S. Kawasaki, H. Isobe, K. Takahashi, Y. Tamakawa and T. Yanagisawa, "Repetitive flash x-ray generator utilizing a simple diode with a new type of energy-selective function," *Rev. Sci. Instrum.*, **61**, 2343-2348, 1990.
7. A. Shikoda, E. Sato, M. Sagae, T. Oizumi, Y. Tamakawa and T. Yanagisawa, "Repetitive flash x-ray generator having a high-durability diode driven by a two-cable-type line pulser," *Rev. Sci. Instrum.*, **65**, 850-856, 1994.
8. E. Sato, K. Takahashi, M. Sagae, S. Kimura, T. Oizumi, Y. Hayasi, Y. Tamakawa and T. Yanagisawa, "Sub-kilohertz flash x-ray generator utilizing a glass-enclosed cold-cathode triode," *Med. & Biol. Eng. & Comput.*, **32**, 289-294, 1994.
9. K. Takahashi, E. Sato, M. Sagae, T. Oizumi, Y. Tamakawa and T. Yanagisawa, "Fundamental study on a long-duration flash x-ray generator with a surface-discharge triode," *Jpn. J. Appl. Phys.*, **33**, 4146-4151, 1994.
10. E. Sato, M. Sagae, E. Tanaka, Y. Hayasi, R. Germer, H. Mori, T. Kawai, T. Ichimaru, S. Sato, K. Takayama and H. Ido: Quasi-monochromatic flash x-ray generator utilizing a disk-cathode molybdenum tube, *Jpn. J. Appl. Phys.*, **43**, 7324-7328, 2004.
11. E. Sato, Y. Hayasi, R. Germer, E. Tanaka, H. Mori, T. Kawai, H. Obara, T. Ichimaru, K. Takayama and H. Ido, "Intense characteristic x-ray irradiation from weakly ionized linear plasma and applications," *Jpn. J. Med. Imag. Inform. Sci.*, **20**, 148-155, 2003.
12. E. Sato, Y. Hayasi, R. Germer, E. Tanaka, H. Mori, T. Kawai, H. Obara, T. Ichimaru, K. Takayama and H. Ido, "Irradiation of intense characteristic x-rays from weakly ionized linear molybdenum plasma," *Jpn. J. Med. Phys.*, **23**, 123-131, 2003.
13. E. Sato, Y. Hayasi, R. Germer, E. Tanaka, H. Mori, T. Kawai, T. Ichimaru, K. Takayama and H. Ido, "Quasi-monochromatic flash x-ray generator utilizing weakly ionized linear copper plasma," *Rev. Sci. Instrum.*, **74**, 5236-5240, 2003.
14. E. Sato, R. Germer, Y. Hayasi, Y. Koorikawa, K. Murakami, E. Tanaka, H. Mori, T. Kawai, T. Ichimaru, F. Obata, K. Takahashi, S. Sato, K. Takayama and H. Ido: Weakly ionized plasma flash x-ray generator and its distinctive characteristics. *SPIE*, **5196**, 383-392, 2003.
15. E. Sato, Y. Hayasi, R. Germer, E. Tanaka, H. Mori, T. Kawai, T. Ichimaru, S. Sato, K. Takayama and H. Ido, "Sharp characteristic x-ray irradiation from weakly ionized linear plasma," *J. Electron Spectrosc. Related Phenom.*, **137-140**, 713-720, 2004.
16. E. Sato, K. Sato and Y. Tamakawa, "Film-less computed radiography system for high-speed imaging," *Ann. Rep. Iwate Med. Univ. Sch. Lib. Arts and Sci.*, **35**, 13-23, 2000.

*obara@rad.cms.tohoku.ac.jp; phone +81-22-717-7941; fax +81-22-717-7944

Heparanase Is Involved in Angiogenesis in Esophageal Cancer through Induction of Cyclooxygenase-2

Takaomi Okawa,[1] Yoshio Naomoto,[1] Tetsuji Nobuhisa,[1] Munenori Takaoka,[1] Takayuki Motoki,[1] Yasuhiro Shirakawa,[1] Tomoki Yamatsuji,[1] Hiroyasu Inoue,[4] Mamoru Ouchida,[2] Mehmet Gunduz,[3] Motowo Nakajima,[5] and Noriaki Tanaka[1]

Abstract **Purpose:** Both heparanase and cyclooxygenase-2 (COX-2) are thought to play critical roles for tumor malignancy, including angiogenesis, although it is unknown about their relationship with each other in cancer progression. We hypothesized that they may link to each other on tumor angiogenesis.

Experimental Design: The expressions of heparanase and COX-2 in 77 primary human esophageal cancer tissues were assessed by immunohistochemistry to do statistical analysis for the correlation between their clinicopathologic features, microvessel density, and survival of those clinical cases. Human esophageal cancer cells were transduced with heparanase cDNA and used for reverse transcription-PCR and Western blot to determine the expression of heparanase and COX-2. COX-2 promoter vector and its deletion/mutation constructs were also used along with transduction of heparanase cDNA for luciferase assay.

Results: Heparanase and COX-2 protein expression exhibited a similar pattern in esophageal tumor tissues, and their expression correlated with tumor malignancy and poor survival. Their expression also revealed a significant correlation with high intratumoral microvessel density. Up-regulation of COX-2 mRNA and protein was observed in esophageal cancer cells transfected with heparanase cDNA. COX-2 promoter was activated after heparanase cDNA was transduced and the deletion/mutation of three transcription factor (cyclic AMP response element, nuclear factor-κB, and nuclear factor-interleukin-6) binding elements in COX-2 promoter strongly suppressed its activity.

Conclusion: Our results suggest that heparanase may play a novel role for COX-2-mediated tumor angiogenesis.

Two essential processes required for metastasis are neoangiogenesis and tumor cell invasion of the basement membrane and extracellular matrix (1). Heparanase specifically cleaves carbohydrate chains of heparan sulfate proteoglycans (HSPG) present in the extracellular matrix and on the cell surface (2). Heparanase has been identified in highly invasive normal and malignant cells, including cytotrophoblasts, activated cells of the immune system, and lymphoma, melanoma, and carcinoma cells (2–8). Normal physiologic functions of heparanase are related to embryonic morphogenesis, wound healing, tissue repair, and inflammation. Enhanced heparanase expression has been reported to correlate with the metastatic potential of human tumor cells (3, 4, 7, 8) and shorter postoperative survival of patients with various cancers (9–12).

Cyclooxygenase-2 (COX-2) is a rate-limiting enzyme involved in the conversion of arachidonic acid to prostaglandin H_2, the precursor of various molecules, including prostaglandins, prostacyclins, and thromboxanes. COX-2 is known to contribute to tumorigenesis and the malignant phenotype of tumor cells in various ways, including (*a*) inhibition of apoptosis (13), (*b*) increased angiogenesis (14), (*c*) increased invasiveness (15, 16), (*d*) modulation of inflammation and immunosuppression (17), and (*e*) conversion of procarcinogens to carcinogens (18, 19). COX-2 converts arachidonic acid to prostaglandins and induces angiogenic factors, such as vascular endothelial growth factor and basic fibroblast growth factor (FGF; refs. 14, 20), and selective inhibitors of COX-2 are effective in inhibition of cancer growth (14, 21). On the other hand, heparanase may also contribute to angiogenesis by cleaving HSPGs and releasing angiogenic factors, such as basic FGF, vascular endothelial growth factor, heparin growth factor, platelet-derived growth factor, and transforming growth factor-β (3, 22–25). Therefore, these two molecules are thought to play

Authors' Affiliations: Departments of [1]Gastroenterological Surgery, Transplant, and Surgical Oncology, [2]Molecular Genetics, and [3]Oral Pathology and Medicine, Graduate School of Medicine and Dentistry, Okayama University, Okayama, Japan; [4]National Cardiovascular Center Research Institute, Osaka, Japan; and [5]Novartis Pharma Tsukuba Institute, Tsukuba, Japan

Received 5/18/05; revised 7/28/05; accepted 8/15/05.

Grant support: Ministry of Education, Culture, Sports, Science, and Technology, Japan grant 13671306.

The costs of publication of this article were defrayed in part by the payment of page charges. This article must therefore be hereby marked *advertisement* in accordance with 18 U.S.C. Section 1734 solely to indicate this fact.

Requests for reprints: Yoshio Naomoto, Department of Gastroenterological Surgery, Transplant, and Surgical Oncology, Graduate School of Medicine and Dentistry, Okayama University, 2-5-1 Shikatacho, Okayama 700-8558, Japan. Phone: 81-86-235-7257; Fax: 81-86-221-8775; E-mail: ynaomoto@md.okayama-u.ac.jp.

©2005 American Association for Cancer Research.

doi:10.1158/1078-0432.CCR-05-1103

a critical role in controlling the invasion and metastasis of malignant tumors. However, the relationship between heparanase and COX-2 has not yet been elucidated.

Esophageal squamous cell carcinoma (ESCC) remains one of the most aggressive malignant tumors, and its prognosis remains worse than those of other gastrointestinal malignancies. The clinical outlook for patients with ESCC is still very poor due to the high rate of local and distant metastasis (26–28). Although conventional pathologic assessment has served as the standard estimation of prognosis of patients with ESCC, it does not always define the individual risk of recurrence after surgical resection. Tumor cell invasion and secondary spread to the blood and lymph vessels are the hallmarks of malignant disease and the greatest impediment to cancer therapy. Recent advances in the molecular genetics of ESCC have stimulated attempts to evaluate the prognostic relevance of specific molecular alterations in the tumor. Identification of a prognostic marker susceptible to or modifiable by direct therapeutic intervention will result in therapeutic and prognostic improvements for these patients.

The present study was designed to map the distribution of heparanase and COX-2 in human esophageal carcinoma using immunohistochemical staining and define the relationship between heparanase/COX-2 and clinicopathologic features. Our findings suggested a positive relationship between heparanase and COX-2 expression, and we therefore elucidated the relationship between heparanase and COX-2 in terms of signal transduction. We attempted to identify transcription factors and transcriptional regulatory elements located in the COX-2 promoter that is activated by heparanase. Based on the additional evidence thus obtained, we propose that the expression of the *COX-2* gene might be regulated by heparanase. This invokes a dynamic relationship with tumor angiogenesis.

Materials and Methods

Patients and tissue sampling. We examined 77 ESCCs, including mucosal carcinomas (n = 6) and submucosal carcinomas (n = 24), obtained from 77 previously untreated patients. The patients included 72 men and 5 women with a mean age of 68.3 years (range, 38-79 years). Tissue samples were surgically resected at the Department of Surgery, Keiyukai Hospital (Sapporo, Hokkaido, Japan) in 1994. Two experienced pathologists, who were blinded to the clinical data and results of other diagnostic tests, determined the grade of dysplasia in all lesions. The clinicopathologic characteristics were evaluated according to the guidelines of the Union Internationale Contre le Cancer. The study protocol was approved by the Human Ethics Review Committee of Okayama University Graduate School of Medicine and Dentistry, and a signed consent form was obtained from each subject.

Cell culture. We used three types of human ESCC cell lines and colon cancer cell lines. Three ESCC cell lines, TE1, TE6, and TE8, were obtained from the Japanese Cancer Research Resource Bank, and T.Tn was obtained from the Japan Cell Research Bank (Ibaraki, Japan). RPMI4788, colon cancer cell line, was kindly provided by the RPMI (Buffalo, NY; ref. 29). These cell lines were propagated in monolayer culture in RPMI 1640 with 25 mmol/L HEPES, 10% FCS, 100 units/mL penicillin, and 100 mg/mL streptomycin at 37°C in a humidified atmosphere of 95% air and 5% CO_2.

Monoclonal antibodies. Anti-human mouse heparanase monoclonal antibody was obtained from Novartis Pharma Tsukuba Institute (Tsukuba, Japan); the monoclonal antibody reacted with both the 65-kDa proform and the 50-kDa mature form of the human heparanase as described previously (9, 30). Monoclonal antibody 13H14 for COX-2 was obtained from IBL (Gunma, Japan). Clone F8/86 for factor VIII–related antigen/von Willebrand factor Ab-2 was obtained from Neo-Markers (Fremont, CA). Antibody for human heparanase was diluted at 1:500. 13H14 was used at a concentration of 3 μg/L and F8/86 was ready to use.

Immunohistochemistry. COX-2 and factor VIII stainings were done using formalin-fixed, paraffin-embedded serial sections. Sections (5 μm thick) were mounted on silanized slides (DAKO Japan Co., Tokyo, Japan), deparaffinized in xylene for 20 minutes, and rehydrated in graded ethanol solutions. Endogenous peroxidase was blocked by incubating the sections in 3.0% H_2O_2 in methanol for 15 minutes. For heparanase and COX-2 staining, antigen retrieval in paraffin sections was done once and thrice, respectively, by heating in 10 mmol/L citrate buffer solution (pH 6.0) in a microwave for 5 minutes. For factor VIII staining, antigen retrieval was done by pepsin (Pepsin solution, Nichirei, Tokyo, Japan) at 37°C for 15 minutes. After blocking of nonspecific reactivity with rabbit serum for 10 minutes at room temperature (Histofine SAB PO kit, Nichirei), sections were incubated overnight at 4°C with the anti-heparanase and anti-COX-2 antibody and for 1 hour at 37°C with anti–factor VIII antibody. Identification of the distribution of the primary antibody was achieved by subsequent application of a biotinylated anti-primary antibody (Histofine SAB PO kit) and streptavidin peroxidase (Histofine SAB PO kit). Immunostaining was developed using 3,3′-diaminobenzidine/H_2O_2 solution (Histofine 3,3′-Diaminobenzidine Substrate kit, Nichirei), and sections were counterstained with Mayer's hematoxylin. As a negative control, some sections were subjected to normal serum blocking and omission of the primary antibody. In each lesion, assessment of heparanase was based on the nuclear or cytoplasmic staining pattern. Assessment of COX-2 was based on the cytoplasmic staining pattern. Expressions of heparanase and COX-2 were considered positive when it stained at the invasive front and tumor edge and was present in >10% of tumor cells. Assessment of factor VIII was based on the expression in vascular endothelial cells.

Evaluation of microvessel density. Evaluation of microvessel density (MVD) was done as described previously (31). Briefly, after microscopic screening for tumor areas of highest MVD at a magnification of ×40, the vessels in five areas with the highest MVD were counted under ×200 magnification by two independent observers blinded to the patient's background. The mean value of the vessel count in five fields by the two observers was considered the MVD for the tumor. Generally, there was no significant interobserver difference, and in cases with wide differences, MVDs were reevaluated by a third observer until the three observers reached a consensus.

Analysis of the relationship between heparanase expression and clinicopathologic factors. Heparanase and COX-2 immunostaining was detected in the cytoplasm of cancer cells. We analyzed the interaction between heparanase/COX-2 expression and clinicopathologic characteristics and evaluated it as a prognostic factor for esophageal cancer patients.

Plasmids and oligonucleotides. Human heparanase cDNA was kindly provided by Dr. Motowo Nakajima (Novartis Pharma Tsukuba Institute), the characteristics of which were described previously (30, 32). Luciferase constructs with the COX-2 promoter (−1,432/+59, −327/+59, −220/+59, −124/+59, −52/+59, KBM, ILM, CRM, KBM-ILM, ILM-CRM, CRM-KBM, and CRM-ILM-KBM) were kind gifts from Dr. Hiroyuki Inoue (National Cardiovascular Center Research Institute, Osaka, Japan; ref. 33). pCRE-Luc, which contains four tandem copies of the nuclear factor-κB (NF-κB) consensus sequence fused to a TATA-like promoter, and pNF-κB-Luc, which contains multiple copies of the cyclic AMP response element (CRE) binding sequence fused to a TATA-like promoter, were purchased from BD Biosciences (San Jose, CA; Mercury Pathway Profiling Luciferase System). pRL-tk, the control luciferase plasmid, was purchased from Promega (Madison, WI).

Transfection. The 3,726-bp-long cDNA coding human *heparanase* gene was inserted into an expression vector, pBK-cytomegalovirus (Stratagene, La Jolla, CA), and directly used for transfection of ESCC cell

lines by LipofectAMINE 2000 reagent (Life Technologies, Gaithersburg, MD). Cells were transfected with 1 μg plasmid DNA in the presence of 10 μL LipofectAMINE 2000 in six-well tissue culture plates containing Opti-MEM reduced-serum medium (Life Technologies). After a 5-hour incubation, the medium was replaced with fresh RPMI 1640 supplemented with 10% fetal bovine serum, 2 mmol/L L-glutamine, 100 units/mL penicillin, and 100 mg/mL streptomycin. For Western blotting, cells were seeded at a density of 2×10^5 per well in six-well dishes and grown to 80% confluence. For each well, plasmid (4 μg; human heparanase cDNA) was introduced into cells using 10 μg LipofectAMINE 2000 according to the manufacturer's instructions. After 12 hours of incubation, the medium was replaced with basal medium. For the luciferase assay, cells were seeded at a density of 5×10^4 per well in 24-well dishes and grown to 50% to 60% confluence. For each well, plasmid DNA (1.0 μg; human heparanase/mock and COX-2 reporter plasmids) was introduced into cells using 3 μg LipofectAMINE 2000 according to the manufacturer's instructions. Luciferase activity was measured in cellular extracts as described below.

Reverse transcription-PCR. Total RNA was isolated from cells using RNAzol (Cinna Biotecx, Friendswood, TX) in a single-step phenol extraction method and used as a template. Reverse transcription was done at 22°C for 10 minutes and then at 42°C for 20 minutes, and PCR was done with specific primers in a volume of 50 μL according to the manufacturer's protocol (PCR kit; Perkin-Elmer/Cetus, Norwalk, CT). The following specific primers were used: heparanase sense (5′-TTCGATCCCAAGGAATCAAC-3′) and antisense (5′-GTAGTGATGC-CATGTAACTGAATC-3′), COX-2 sense (5′-GGGTTGCTGGGGGAA-GAAATGTG-3′) and antisense (5′-GGTGGCTGTTTTGGTAGGCTGTG-3′), and glyceraldehyde-3-phosphate dehydrogenase sense (5′-CAGCC-GAGCCACATC-3′) and antisense (5′-TGAGGCTGTTGTCATACTTCT-3′). For heparanase, the amplification reaction involved denaturation at 95°C for 45 seconds, annealing at 60°C for 1 minute, and extension at 72°C for 1 minute; for COX-2, the amplification reaction involved denaturation at 94°C for 45 seconds, annealing at 60°C for 45 seconds, and extension at 72°C for 1 minute using a thermal cycler (Perkin-Elmer, Foster City, CA). The PCR products were applied on 1% agarose gels and visualized by SYBR Gold (Molecular Probes, Eugene, OR) staining.

Quantitative real-time reverse transcription-PCR. Heparanase mRNA copy number in cell lines was determined by quantitative real-time reverse transcription-PCR using a LightCycler instrument and a Light-Cycler DNA Master SYBR Green I kit (Roche Molecular Biochemicals, Indianapolis, IN). Amplifications were done in glass capillary tubes using 20 μL reaction containing 3 mmol/L $MgCl_2$, 0.5 μmol/L of each primer, and 2 μL of 10× LightCycler FastStart DNA Master SYBR Green I. PCR amplification began with a 60-second denaturation step at 95°C followed by 40 cycles of denaturation at 95°C for 15 seconds, annealing at 58°C for 10 seconds, and extension at 72°C for 9 seconds. The oligonucleotides used as specific primers were 5′-GCGGTTACCC-TATCCTTTTT-3′ and 5′-GCAGCAACTTTGGCATTTC-3′. Copy numbers of mRNA were calculated from serially diluted standard curves generated from purified cDNA template, which consisted of a human heparanase cDNA of 1,758 bp inserted into the expression vector. Data analysis was done using LightCycler Software (Roche Molecular Biochemicals).

Western blotting. Cells were collected by trypsinization and washed twice in cold PBS. Cells then were dissolved in lysis buffer containing 20 mmol/L Tris-HCl (pH 7.6), 150 mmol/L NaCl, 1 mmol/L $CaCl_2$, 1 mmol/L $MgCl_2$, 1% NP40, 10% glycerol, and protease inhibitors (1 mmol/L phenylmethylsulfonyl fluoride, 1 mmol/L DTT, 20 μg/mL aprotinin, and 20 μmol/L leupeptin). Lysis was carried out at 4°C for 30 minutes and lysates were centrifuged at 15,000 rpm for 20 minutes. The protein concentration of the supernatant was determined using the Bio-Rad Protein Assay (Bio-Rad, Hercules, CA). Equal amounts (40 μg) of proteins were electrophoresed under reducing conditions on 12% (w/v) polyacrylamide gels. Proteins were electrophoretically transferred to Hybond polyvinylidene difluoride transfer membranes (Amersham, Arlington Heights, IL) and incubated with primary antibodies against COX-2 and heparanase and then peroxidase-linked secondary antibody. An Amersham Enhanced Chemiluminescence Western System (Amersham, Tokyo, Japan) was used to detect secondary probes.

Luciferase assay. Reporter plasmids containing the 327-bp flanking region of the human COX-2 promoter with deletion or site-specific mutation are represented schematically in Fig. 5A and B. Relative positions of the NF-κB site, nuclear factor-interleukin-6 (NF-IL6) site, and the CRE are indicated. Heparanase cDNA expression vector was transiently transfected with each reporter plasmid together with pRL-tk used as an internal control for the Dual-Luciferase Reporter Assay System (Promega). The cells were then harvested, lysed, and assayed for luciferase activity. Luciferase activity was measured by Luminoskan (Labsystems, Helsinki, Finland). Results are represented as relative luciferase activities normalized by dividing with the luciferase activity using the empty vector (mock). Data are mean ± SD of four individual experiments.

Statistical analysis. Heparanase expression was assessed for association with clinicopathologic variables and COX-2 expression using the χ^2 two-tailed test, Fisher's exact test, and Spearman's correlation coefficient test. Survival analysis was calculated using the Kaplan-Meier method and compared by the Wilcoxon test. $P < 0.05$ denotes the presence of a statistically significant difference. Differences of MVD between heparanase-positive and heparanase-negative tumors were examined using the unpaired t test. The rate of double-stained cells was assessed using the two-tailed test.

Results

Distribution of heparanase and cyclooxygenase-2 in normal and cancer tissues of the esophagus. Heparanase was barely detectable in normal esophageal tissue (34, 35). However, in the stromal compartment adjacent to tumor tissue, vascular endothelial cells and fibroblasts as well as inflammatory cells, such as macrophages, lymphocytes, and neutrophils, stained strongly for heparanase (Fig. 1A and B). Heparanase expression was also observed in dysplastic areas. Severe and moderate dysplasia was associated with stronger heparanase expression than that seen in mild dysplasia as we have shown previously (35). With respect to invasive tumors, heparanase and COX-2 were expressed in the cytoplasm and cell surface of carcinoma cells at the tumor edge and invasive front, respectively (Fig. 1B and D). Heparanase exhibited progressively stronger expression in lesions from dysplasia through invasive cancer of the esophagus. Metastatic lymph nodes had less or an equal level of heparanase expression in comparison with their primary lesions (35).

COX-2 staining was not detected in normal esophageal tissues (data not shown). Inflammatory cells and vascular endothelial cells in stromal tissue adjacent to tumor tissues showed strong COX-2 expression similar to the pattern observed for heparanase (Fig. 1C and D). In addition, COX-2 expression in esophageal carcinomas was evident as the cells progressed from dysplasia to invasive squamous carcinoma (data not shown). In advanced cancer tissues, COX-2 protein immunoreactivity was diffusely present in the cytoplasm. COX-2 expression exhibited a very similar pattern to that of heparanase expression in esophageal cancer tissues (Fig. 1C and D).

Relationship between heparanase/cyclooxygenase-2 expression and clinicopathologic factors. Because COX-2 and heparanase have been known as bad prognostic markers in various cancers due to their contribution to cancer invasion and metastasis, and the current similar expression pattern in our samples was

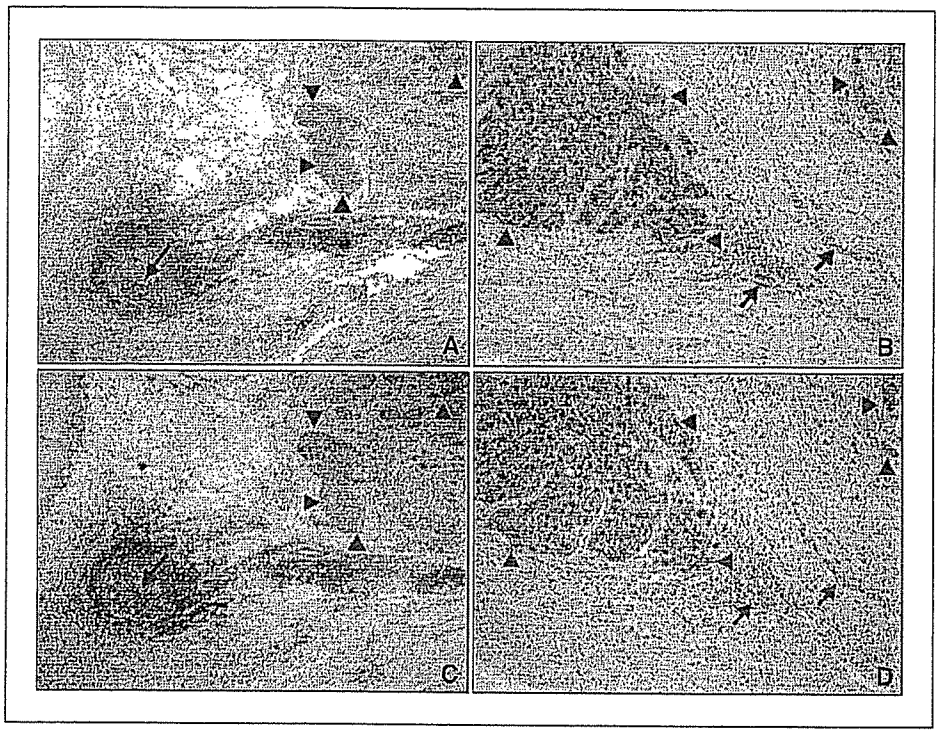

Fig. 1. Immunohistochemical analysis of the heparanase (*A* and *B*) and COX-2 (*C* and *D*) proteins in esophageal tissues. Stromal tissues around tumor tissue are both heparanase and COX-2 positive (*A* and *C*, respectively), whereas neither heparanase nor COX-2 was expressed in normal epithelium. Strong staining of heparanase and COX-2 was also detected at the invasive front in cancer tissue (*B* and *D*, respectively). Original magnifications, ×200 (*A* and *C*) and ×400 (*B* and *D*). Tumor cells at the invasive front were strongly stained with heparanase and COX-2 (*A-D, arrowheads*). Inflammatory cells (*B* and *D*) and the cells in the lymph follicle (*A* and *C*) were also stained with heparanase and COX-2 (*arrows*).

observed, we examined such relationship of both molecules in the same samples. Figure 2A-D shows immunohistochemical analysis for heparanase and COX-2. Figure 2A and C shows positive analysis for heparanase and COX-2, and Fig. 2B and D shows negative analysis for heparanase and COX-2. Fifty-three of the 77 (68.8%) ESCC cases stained positively for heparanase and 56 of 77 (72.7%) stained positively for COX-2. The relationship between heparanase/COX-2 expression and clinicopathologic characteristics is shown in Table 1. With respect to depth of invasion, all cases of carcinoma *in situ* were heparanase negative. Heparanase and COX-2 immunoreactivity increased gradually from T_1 to T_4 stage tumors. All T_4 lesions were both heparanase positive and COX-2 positive. Both heparanase and COX-2 were correlated significantly with invasion depth (P = 0.0018 and 0.0209, respectively). Thirty-two of 40 (80.0%) tumors with lymph node metastasis were positive for heparanase expression, and heparanase was negative in 16 of 37 (43.2%) tumors without lymph node involvement (P = 0.0278). COX-2 expression was also significantly correlated to lymph node metastasis (P = 0.0453). Of the tumors with lymph node metastasis, 32 cases were positive for both heparanase and COX-2. Heparanase staining gradually increased from stage 0 to 4 (P = 0.0406). Of the stage IV tumors, 70.0% exhibited positive staining, whereas only 1 of 5 (20%) was positive for heparanase at stage 0. Heparanase and COX-2 were detected in 31 cases of 36 (86.1%) tumors with lymphatic invasion, and 19 of 41 (46.3%) and 16 (40.2%) of 41 tumors without lymphatic invasion were negative for heparanase and COX-2, respectively (P = 0.0029 and 0.00202, respectively). Of the tumors with lymphatic invasion, 27 cases were positive for both heparanase and COX-2. These results suggest that both heparanase and COX-2 expressions in ESCC are closely involved in tumor invasion and metastasis.

We examined the survival in relation to heparanase and COX-2 expression. Seventy-five percent and 76.2% of patients with tumors negative for heparanase and COX-2, respectively, survived, whereas the survival rate was 33.7% and 35.7% in patients with heparanase and COX-2 immunopositivity 5 years after surgery (P = 0.0005 and 0.0009, respectively; Fig. 2E).

Expression of heparanase and cyclooxygenase-2 predicts neovascularization of esophageal cancer. Microvessels in tumor tissue were detected by immunohistochemical analysis using anti-factor VIII antibody. Figure 3C shows microvessels in tumor tissue. Heparanase and COX-2 were expressed in microvessels in tumor tissue (Fig. 3A and B, respectively). The MVD in the esophageal cancers ranged from 0 to 34.8 (18.6 ± 8.6, mean ± SD). Based on the mean value of the MVD for all tumors, esophageal cancers were divided into two groups: high MVD group (MVD ≥ 18.6; n = 43) and low MVD group (MVD < 18.6; n = 34; Table 2A). The number of the patients who showed high MVD was significantly associated with heparanase positive and COX-2 positive tumors (P = 0.0001 and 0.0002, respectively). Heparanase-positive tumors had a significantly higher vascularity (MVD 21.4 ± 6.5) compared with heparanase-negative tumors (MVD, 12.2 ± 7.9; P < 0.0001; Table 2B). Tumors with positive COX-2 expression also had a significantly higher MVD (20.9 ± 6.7) compared with those negative for COX-2 (12.2 ± 8.3; P < 0.0001; Table 2B). Combination of heparanase-positive and COX-2-positive expression was also significantly associated with higher MVD (Fig. 3D). The high MVD group exhibited a significantly worse survival rate (33.3%) than the low MVD group (P = 0.0021; Fig. 3E).

Comparison of heparanase and cyclooxygenase-2 expression. In both superficial carcinomas and advanced ESCCs, COX-2 expression correlated significantly with heparanase expression (Table 2C). Fifteen of 29 (51.7%) cases with early-stage cancers

were negative for both COX-2 and heparanase. On the other hand, of advanced tumors (stage T_2-T_4), 41 of 48 (85.4%) cases were positive for both COX-2 and heparanase. Interestingly, in this study, no cases were found to be heparanase positive and COX-2 negative. All of the heparanase-positive cases were also COX-2 positive. In addition, 3 of 77 (3.9%) cases were heparanase negative but COX-2 positive. These findings suggested that heparanase is strongly linked to COX-2 expression.

Heparanase up-regulates cyclooxygenase-2 mRNA and protein in human esophageal cancer cells. To analyze the relationship between heparanase and COX-2, we first examined heparanase and COX-2 protein expression by Western blotting in three ESCC cell lines (TE1, TE8, and T.Tn). All cell lines showed low-level heparanase protein expression (Fig. 4A, *lanes 1, 4,* and *7*). COX-2 protein was also showed a low expression in these cell lines. The mRNA levels of both genes were also low in all cell lines (Fig. 4B, *lane 1* for T.Tn; data not shown for TE1 and TE8). Therefore, we transfected the heparanase cDNA expression vector into the cell lines and confirmed that the heparanase mRNA and protein showed an increased expression (Fig. 4A, *lanes 3, 6,* and *9*; Fig. 4B, *lane 3*). Notably, we found that the COX-2 mRNA and protein were enhanced in the heparanase-transfected cell lines compared with the empty vector (mock)-transfected cells and parental cell lines, although COX-1 expression was not changed by heparanase (Fig. 4A and B). When we used RPMI4788, a colon cancer cell line that exhibited lower-level COX-2 expression and no heparanase expression, an increased COX-2 mRNA in the heparanase-transfected RPMI4788 cells was detected (Fig. 4B, *lane 6*). Furthermore, the increase of the *COX-2* gene expression was confirmed in the T.Tn cells by real-time PCR (Fig. 4C) after transfection of the heparanase expression vector. These data suggest that the COX-2 expression is up-regulated through the heparanase induction

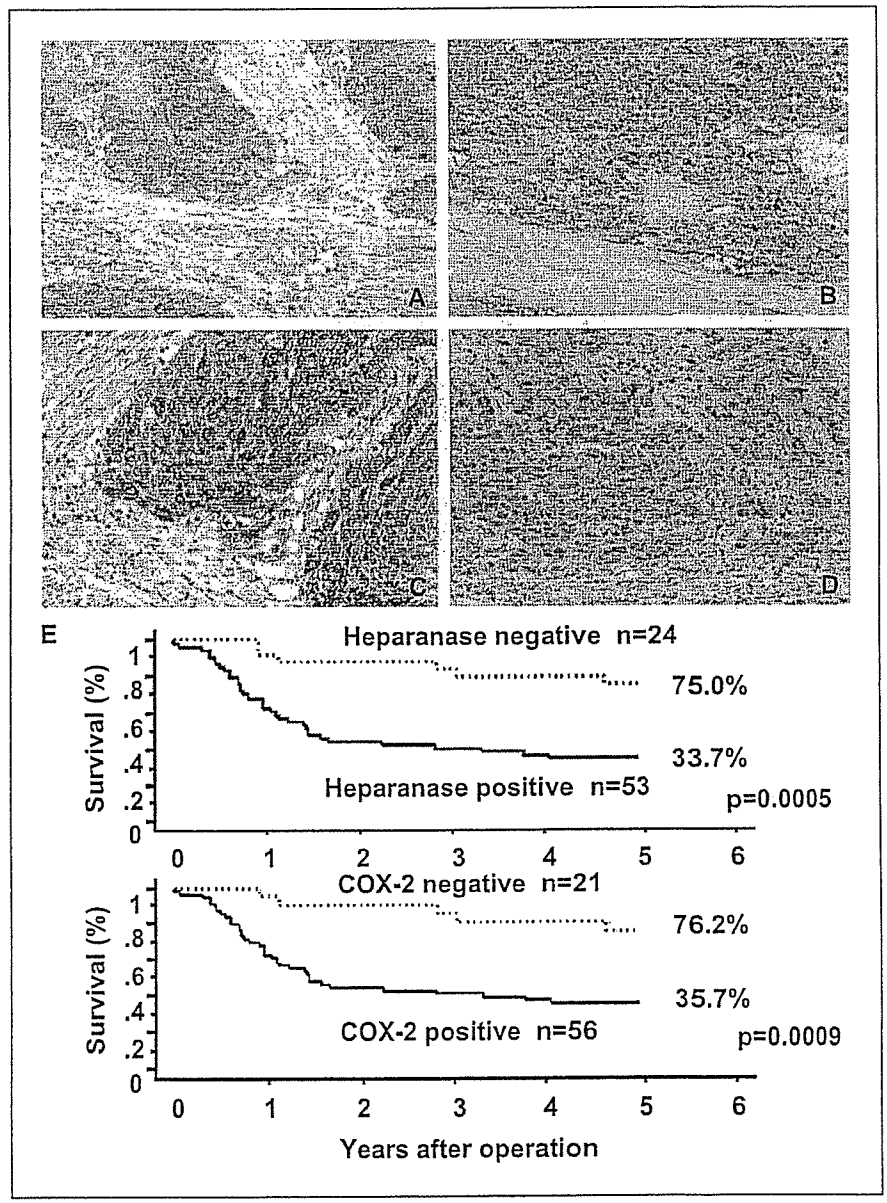

Fig. 2. Intracellular heparanase and COX-2 staining patterns in tumor cells (*A-D*). Positive staining for heparanase (*A*) and COX-2 (*C*) in the cytoplasm. Negative staining for heparanase (*B*) and COX-2 (*D*) in the cytoplasm. Original magnification, ×400. *E*, Kaplan-Meier survival curves of patients with esophageal carcinomas with respect to heparanase or COX-2 expression status. Both heparanase-positive patients and COX-2-positive patients exhibit significantly poorer survival rates compared with each group of patients who are negative.

Table 1. Relationship between heparanase or COX-2 expression and clinicopathologic variables in ESCCs

	Heparanase			COX-2		
	Negative	Positive	*P*	Negative	Positive	*P*
Differentiation						
Well	9	31	0.128	7	33	0.072
Moderate	14	18		13	19	
Poor	1	4		1	4	
Depth						
T_{is}	3	0	0.0018	2	1	0.0209
T_{1a}	2	1		2	1	
T_{1b}	12	12		11	13	
T_2	1	11		1	11	
T_3	6	25		5	26	
T_4	0	4		0	4	
Lymph node metastasis						
N_0	16	21	0.0278	14	23	0.0453
N_1	8	32		7	33	
Distant metastasis						
M_0	21	46	0.89	18	49	0.88
M_{1a}	3	5		3	5	
M_{1b}	0	2		0	2	
Stage						
0	4	1	0.0406	3	2	0.0652
I	8	7		8	7	
IIa	4	11		3	12	
IIb	3	11		2	12	
III	2	16		2	16	
IVa	2	5		2	5	
IVb	1	2		1	2	
Lymph vessel invasion						
(−)	19	22	0.0029	16	25	0.0202
(+)	5	31		5	31	
Vascular invasion						
(−)	24	47	0.169	21	50	0.181
(+)	0	6		0	6	

NOTE: (−) and (+), absence and presence, respectively, of lymph and vascular invasions.

in esophageal cancer cell lines. We further examined the gene regulation using a COX-2 promoter luciferase construct (36, 37). After cotransfection of luciferase reporter plasmid containing the longest promoter (−1,432 to +59) of the *COX-2* gene with the heparanase cDNA expression vector or empty vector (mock), the heparanase-transfected TE1, TE8, T.Tn, and RPMI4788 cells exhibited 1.87-, 1.85-, 1.74-, and 2.56-fold increases in luciferase activity compared with mock, respectively (Fig. 4D).

Identification of the cyclooxygenase-2 promoter region regulated by human heparanase. Based on earlier reports about the COX-2 transcriptional mechanism (33, 38), we hypothesized that heparanase might regulate the *COX-2* gene at the transcriptional level and that the *COX-2* is a downstream target gene of heparanase. To test this hypothesis, we used RPMI4788 cell line to analyze the heparanase-responsible regions on the COX-2 promoter. We did cotransfection of heparanase expression vector with a series of luciferase reporter plasmids that have the COX-2 promoter, encompassing the regions of −327 to +59, −220 to +59, −124 to +59, and −52 to +59 (Fig. 5A). The −327 to +59, −224 to +59, and −124 to +59 promoter regions showed 2.23-, 2.25-, and 3.28-fold increases of luciferase activity in RPMI4788 cells, respectively. However, the −52 to +59 COX-2 promoter exhibited less luciferase activity (Fig. 5B, *lanes 1-4*). Using TE8 cell line, the heparanase response pattern of the COX-2 promoter was similar to that of RPMI4788 cells, whereas the luciferase activities were low (Fig. 5B, *lanes 5-8*).

Furthermore, to define the responsible elements for heparanase in the COX-2 promoter, we used mutant forms (mNF-κB, mNF-IL6, and mCRE) of NF-κB, NF-IL6, and CRE binding elements on the COX-2 promoter containing −327 to +59 region (Fig. 6A). As shown in Fig. 6C, mNF-κB, mNF-IL6, and mCRE exhibited 2.44-, 2.16-, and 2.57-fold luciferase activity, respectively. These activities were almost same as that of the normal promoter containing −327 to +59 region (*lane1*; 2.47-fold). Next, we used double-mutant COX-2 promoter plasmids, which are mNF-κB/mCRE, mNF-κB/mNF-IL6, and mNF-IL6/

mCRE (Fig. 6A). The relative luciferase activities are 2.16-fold in mCRE/mNF-κB, 1.93-fold in mNF-κB/mNF-IL6, and 1.27-fold in mNF-IL6/mCRE. The cells transfected with triple-mutant (mNF-κB/mNF-IL6/mCRE) showed 0.80-fold luciferase activity (Fig. 6C). These results suggested that CRE, NF-κB, and NF-IL6 binding elements are all involved in the transcriptional activation of the COX-2 promoter mediated by heparanase, although the effect is not synergistic. Therefore, we used the other luciferase plasmids, pCRE-Luc and pNF-κB-Luc, which have multiple copies of CRE and NF-κB consensus binding elements, respectively (Mercury Pathway Profiling Luciferase System; Fig. 6B). Cells transfected with pNF-κB-Luc or pCRE-Luc showed 3.77- and 3.95-fold luciferase activity, respectively (Fig. 6C). These results suggest that heparanase increases the transcriptional activity of the COX-2 promoter and that this effect is likely to be dependent on all CRE, NF-κB, and NF-IL6 binding sites.

Discussion

Our results showed that heparanase and COX-2 are closely correlated with tumor malignancy through angiogenesis and that heparanase regulates the COX-2 expression. Immunohistochemical analysis revealed that heparanase and COX-2 proteins show very similar expression profile in esophageal cancer tissues, especially in tumor cells and stromal cells, such as fibroblasts, vascular endothelial cells, and inflammatory cells. Heparanase and COX-2 expression were located in the cytoplasm of tumor cells and highly correlated with depth of tumor invasion, lymph node metastasis, and lymphatic invasion. These findings support the notion that heparanase and COX-2 are involved in invasion and metastasis of malignant cells. Previous studies have shown that heparanase expression in esophageal cancer was significantly correlated with clinicopathologic variables and loss of syndecan-1 (34). In addition, the prognosis of patients with heparanase-positive and COX-2-positive tumors was significantly poorer than that of those with heparanase-negative and COX-2-negative tumors (3, 9, 12, 39). These results suggest that COX-2, as well as heparanase, is associated with tumor progression and prognosis in esophageal cancer.

Heparanase and COX-2 were also expressed strongly in stromal tissues adjacent to tumor tissues, such as vascular endothelial cells in angiogenic sprouts, fibroblasts, and inflammatory cells. Friedmann et al. (40) used immunohistochemical staining of human colon carcinoma tissue to show high expression of the heparanase protein in the endothelium of angiogenic sprouting capillaries but not of mature quiescent vessels. Masferrer et al. (41) showed that COX-2 immunoreactivity is associated with the microvasculature. These findings suggested that both heparanase and COX-2 are very important for cell-extracellular matrix interaction and that they may contribute to cancer progression. Therefore, we hypothesized that heparanase and COX-2 are linked to extracellular moieties and events, especially tumor angiogenesis. Tumor growth and

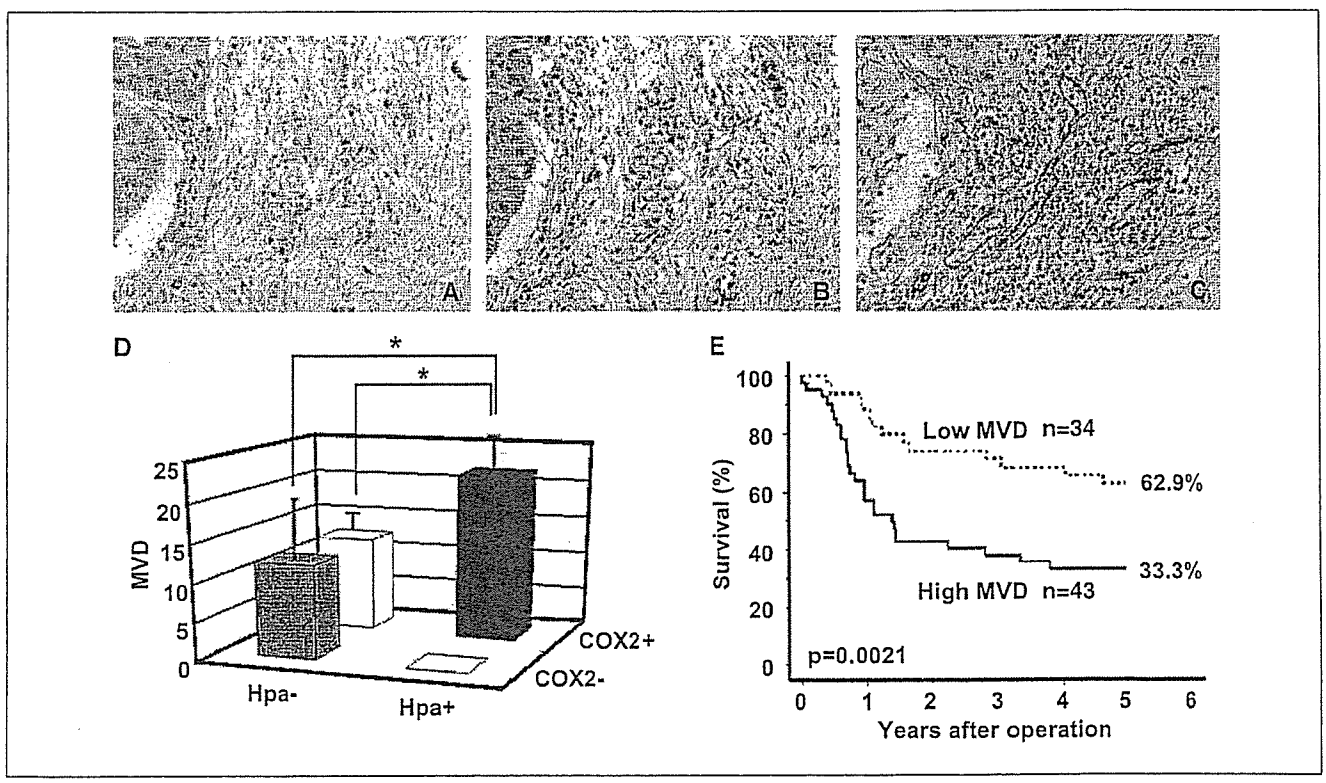

Fig. 3. Heparanase and COX-2 are expressed in vascular sprouts in intratumor tissue (*A* and *B*, respectively). Microvessels in tumor tissues detected by immunohistochemistry using anti-human von Willebrand factor (factor VIII) antibody (*C*). *D*, microvessel count in esophageal cancer according to expression of heparanase (*Hpa*) and COX-2. The MVD is shown against the heparanase and COX-2 expressions. *, $P < 0.005$. *E*, Kaplan-Meier survival curve of esophageal carcinoma patients with respect to MVD. High MVD patients show poor survival.

Table 2. Relationship with heparanase and COX-2 expression

A. Case no. in high and low MVD groups

	Low MVD (<18.6)*	High MVD (≥18.6)*	P
Heparanase (−)	20	4	0.0001
Heparanase (+)	14	39	
COX-2 (−)	17	4	0.0002
COX-2 (+)	17	39	

B. Mean value of MVD

	MVD†	P
Heparanase (−)	12.24 ± 7.85	<0.0001
Heparanase (+)	21.39 ± 6.45	
COX-2 (−)	12.21 ± 8.32	<0.0001
COX-2 (+)	20.90 ± 6.71	

C. Stage of esophageal squamous carcinomas

	Heparanase (−)	Heparanase (+)	P
T_{is}-T_{1b}			
COX-2 (−)	15	0	<0.0001
COX-2 (+)	2	12	
T_2-T_4			
COX-2 (−)	6	0	<0.0001
COX-2 (+)	1	41	
Total			
COX-2 (−)	21	0	<0.0001
COX-2 (+)	3	53	

NOTE: (−) and (+), absence and presence, respectively, of heparanase and COX-2 immunostainings.
*Mean MVD for all tumors was 18.6 ± 8.6.
†Mean ± SD.

metastasis depend on angiogenesis, which results from a cascade of molecular and cellular events that are involved n cell-extracellular matrix interactions (42). Degradation of extracellular matrix by matrix metalloproteinases and heparanase is a key process in cancer progression and facilitates neoangiogenesis. An important step in the angiogenic cascade is degradation of the subendothelial capillary basement membrane by proliferating endothelial cells, a prerequisite for the formation of vascular sprouts. HSPGs are prominent components of blood vessels. After degradation of HSPGs by heparanase, many angiogenic factors, such as basic FGF, transforming growth factor-β, heparin growth factor, and vascular endothelial growth factor, are released and activated. Elkin et al. (23) reported that recombinant heparanase released an active form of basic FGF and increased the angiogenic response. On the other hand, COX-2 is a rate-limiting enzyme involved in the conversion of arachidonic acid to prostaglandin H_2. The eicosanoids, especially prostaglandin E_2, are tightly associated with neovascularization and support vasculature-dependent solid tumor growth and metastasis. The tumorigenic effects of COX-2 could be divided into two distinct groups: the direct effect on tumor cells and the effect on nontumor cells, such as tumor-nurturing blood vessels and immunocompetent cells (43). Jones et al. (21) also showed that COX-2 inhibitors inhibited angiogenesis via direct effects in endothelial cell lines and that COX-2 was important for the direct regulation of angiogenesis in endothelial cells. Recent evidence has showed that COX-2 modulates angiogenesis either by augmenting the release of vascular endothelial growth factor, basic FGF, and nitric oxide by the tumor cells or by directly increasing production of prostaglandins (14, 44). In the present study, we analyzed MVD because it has been reported that heparanase and COX-2 are involved in angiogenesis as reflected by MVD (31, 39, 45). As shown in Fig. 3, in esophageal cancer patients, COX-2 and heparanase independently showed significant higher MVD. However, the immunopositivity of both heparanase and COX-2 showed the highest MVD, suggesting their additive function on angiogenesis. On the other hand, none of the heparanase-positive tumors were negative for COX-2, suggesting the inductive effect of heparanase on COX-2. Therefore, both heparanase and COX-2 might facilitate tumor angiogenesis, and these molecules might interact with each other. How does heparanase interact with COX-2? These two molecules showed similar expression pattern in both early and advanced stages of ESCCs significantly (Table 2C). The COX-2 mRNA and protein were up-regulated in heparanase-transfected esophageal cancer cells (Fig. 4). Therefore, we hypothesized that COX-2 acts downstream of heparanase and that the COX-2 promoter may contain heparanase-responsive regions.

COX-2 expression is differently regulated in various types of the cells (46) and also plays a key role in tumorigenesis (47). The COX-2 promoter contains three known consensus sequences for NF-κB, NF-IL6, and CRE, which are differently involved in the COX-2 promoter activity in different cells (37, 38, 48). In this study, we showed that combination of the CRE, NF-κB, and NF-IL6 site in the human *COX-2* gene was involved in promoter activity. Triple mutant (mNF-κB/mNF-IL6/mCRE) revealed remarkably reduced luciferase activity, whereas the destruction of the CRE, NF-κB, or NF-IL6 site alone showed no significant effect (Fig. 6C). The COX-2 promoter luciferase vectors containing double mutants of these sites also showed reduced promoter activity mediated by heparanase (Fig. 6C), although we could not exclude the possibility that the CRE, NF-κB, and NF-IL6 sites modulate the basal rather than the inducible promoter activity. It was reported that transcriptional regulation might be achieved through the cooperation of more than one *trans*-acting factor with the regulated assembly of multiprotein complexes on enhancers and promoters (49). The complex nature of these processes is thought to result in an elaborated fail-safe mechanism for controlling gene expression (49). Our results may be explained by the fail-safe mechanism of gene expression resulting from complex formation between transcription factors through the CRE, NF-κB, and NF-IL6 sites and other *cis*-acting element(s). Indeed, the promoter activity with mCRE and mNF-κB was increased as little as 2.57- and 2.44-fold, respectively, although those with multiple copies of CRE and NF-κB were increased ~3.95- and 3.77-fold, respectively (Fig. 6C). Based on these results, we inferred that NF-IL6 might be a component of a transcription factor

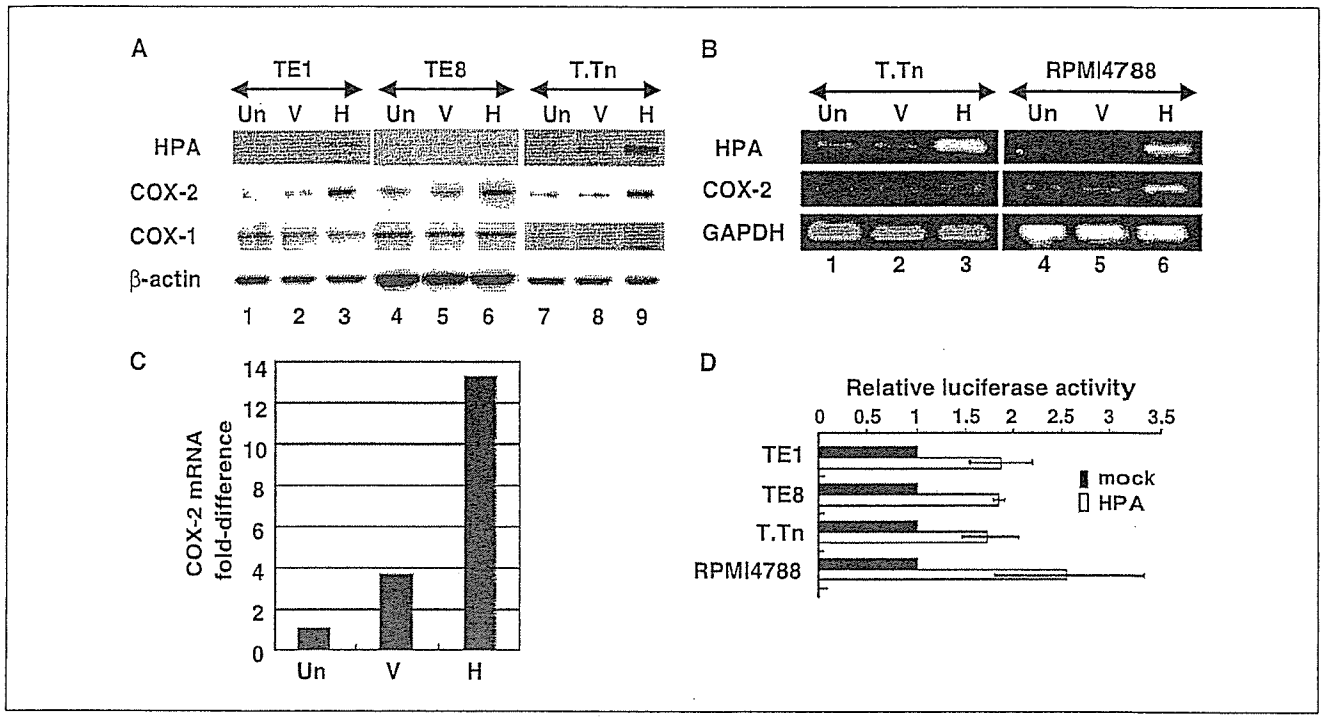

Fig. 4. Heparanase up-regulates COX-2 expression in cancer cell lines. *A*, Western blotting of esophageal squamous cancer cell lines, TE1 (*lanes 1-3*), TE8 (*lanes 4-6*), and T.Tn (*lanes 7-9*). COX-1 protein is shown as an internal control. *B*, heparanase cDNA-transfected T.Tn cells (*lane 3*) and RPMI4788 (*lane 6*) show increased COX-2 mRNA in comparison with parental and mock control (*lanes 1* and *2* for T.Tn and *lanes 4* and *5* for RPMI4788, respectively). *C*, up-regulation of the COX-2 mRNA in heparanase cDNA-transfected T.Tn cells by real-time PCR at 48 hours after transfection. The value in untransfected T.Tn cells is shown as 1. Un, untransfected cells; V, empty vector-only transfected cells; H, heparanase cDNA-transfected cells. *D*, relative luciferase activity is evaluated in TE1, TE8, T.Tn, and RPMI4788 cell lines using luciferase plasmid with COX-2 promoter (−1,432 to −59). Luciferase activity using empty vector (*mock*) is shown as 1. Each cell line shows higher luciferase activity in heparanase-transfected cells (*white columns*) than in mock control (*black columns*).

complex, which increased the COX-2 promoter activity mainly via the CRE and NF-κB, and that the increased promoter activity induced by the CRE and NF-κB might be finely regulated by other transcription factor(s) via the NF-IL6 site or other *cis*-acting element(s). The NF-IL6 site may be a candidate for such a *cis*-acting element, because NF-IL6 has been isolated as a *trans*-acting factor that binds to the p50 subunit of NF-κB (50). Our results using a series of truncated COX-2 promoters also suggest the existence of negative regulatory region on the −220 to −125 of the promoter. How the transcriptional regulation might work? Does heparanase bind directly to these sites or regulate other

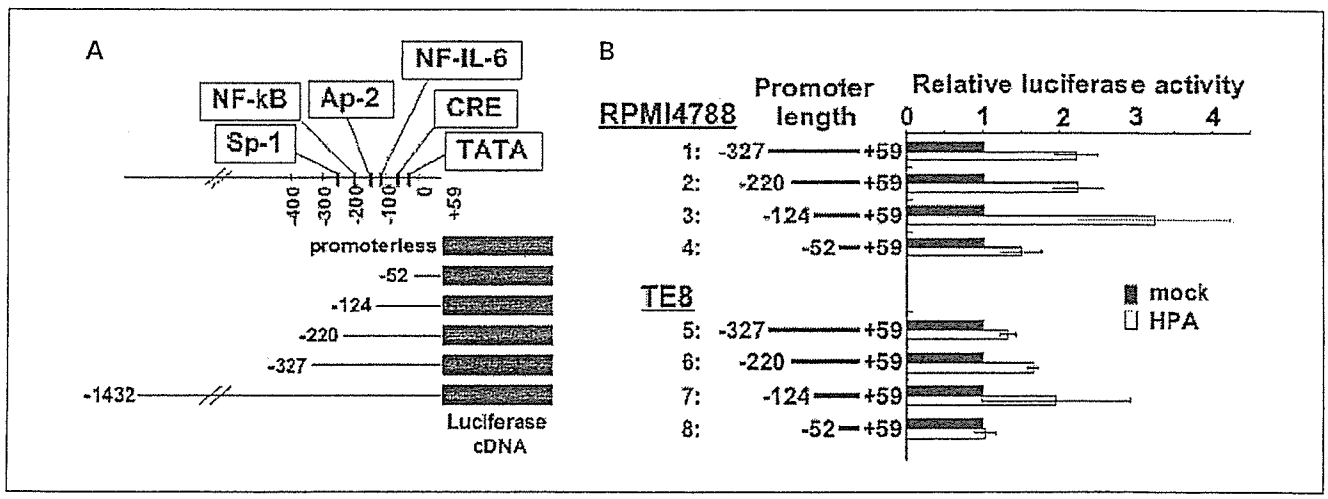

Fig. 5. *A*, schematic representation of reporter plasmids containing the human COX-2 promoter with truncation. *B*, transcriptional activity of the COX-2 promoters containing the regions of −327 to +59 (*lanes 1* and *5*), −224 to +59 (*lanes 2* and *6*), −120 to +59 (*lanes 3* and *7*), and −55 to +59 (*lanes 4* and *8*) in RPMI4788 cells (*lanes 1-4*) and TE8 cells (*lanes 5-8*).

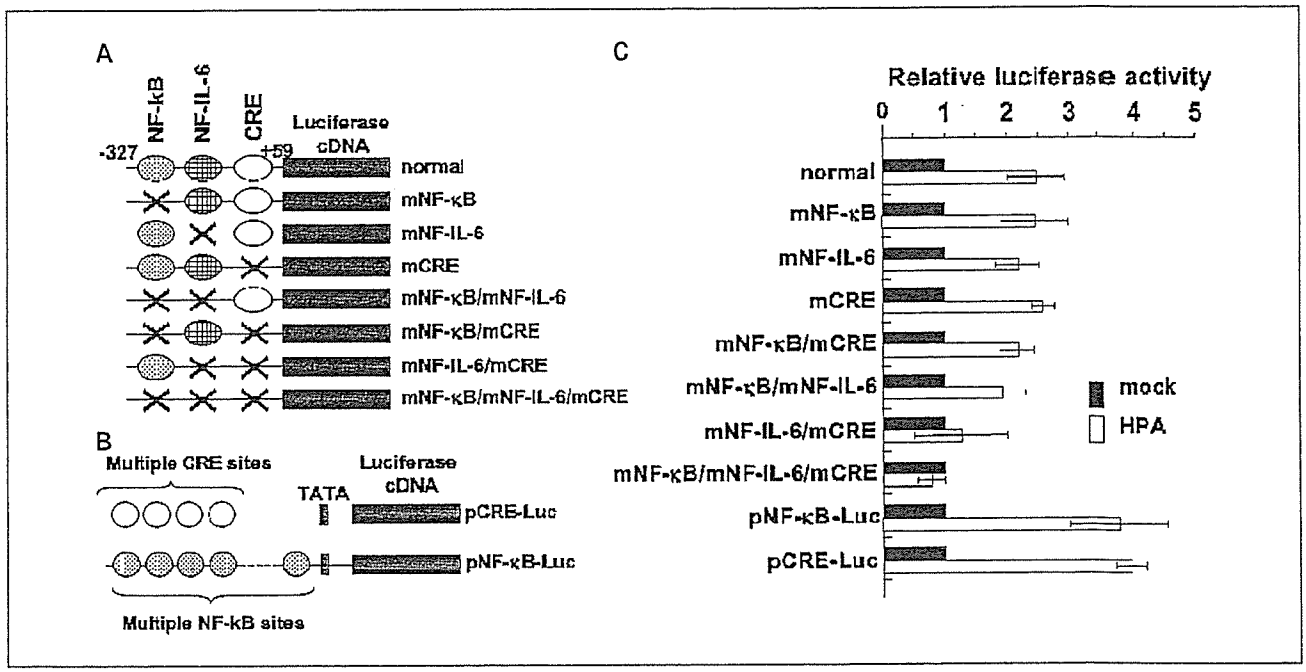

Fig. 6. *A* and *B*, schematic representation of reporter plasmids containing the mutant COX-2 promoters and consensus elements for NF-κB, mNF-IL6, and CRE (*A*) as well as pCRE-Luc and pNF-κB-Luc (*B*). The COX-2 promoter region (−327 to +59) was used for normal control (*lane 1*). *C*, relative luciferase activity. Columns, mean of four individual experiments; bars, SD.

molecules, which are linked to these transcription binding sites? We and others identified recently that the nuclear localization of heparanase and the presence of HSPGs in the nucleus are already known (35, 51). A recent study showed that nuclear heparanase degrades nuclear HSPGs, which may affect the transcriptional activity associated with FGF-2 (51). Although we currently do not have any direct or indirect proof about the relationship between heparan sulfate and the activities of transcriptional sites observed in our study, further analysis will clarify this point.

In conclusion, we showed that heparanase and COX-2 were tightly correlated with MVD and clinicopathologic features in esophageal cancers and that the COX-2 expression is up-regulated by heparanase. The expression pattern of the human *COX-2* gene is primarily accounted for by the transcriptional activity of the 5′ flanking region. The NF-κB and CRE sites were shown to be cooperatively involved in the *COX-2* gene promoter activity mediated by heparanase, although other *cis*-acting element(s), such as NF-IL6, may also be involved in this inducible promoter activity. Further analyses will be required to make clear the transcriptional mechanisms that are involved in activation of the COX-2 promoter by heparanase and their roles in tumorigenesis of esophageal cancers.

References

1. Eccles SA. Heparanase: breaking down barriers in tumors. Nat Med 1999;5:735–6.
2. Nakajima M, Irimura T, Di Ferrante N, Nicolson GL. Metastatic melanoma cell heparanase. Characterization of heparan sulfate degradation fragments produced by B16 melanoma endoglucuronidase. J Biol Chem 1984;259:2283–90.
3. Vlodavsky I, Friedmann Y, Elkin M, et al. Mammalian heparanase: gene cloning, expression and function in tumor progression and metastasis. Nat Med 1999;5: 793–802.
4. Hulett MD, Freeman C, Hamdorf BJ, Baker RT, Harris MJ, Parish CR. Cloning of mammalian heparanase, an important enzyme in tumor invasion and metastasis. Nat Med 1999;5:803–9.
5. Parish CR, Freeman C, Hulett MD. Heparanase: a key enzyme involved in cell invasion. Biochim Biophys Acta 2001;1471:M99–108.
6. Nakajima M, Irimura T, Nicolson GL. Heparanases and tumor metastasis. J Cell Biochem 1988;36: 157–67.
7. Nakajima M, Irimura T, Di Ferrante D, Di Ferrante N, Nicolson GL. Heparan sulfate degradation: relation to tumor invasive and metastatic properties of mouse B16 melanoma sublines. Science 1983;220:611–3.
8. Vlodavsky I, Ishai-Michaeli R, Mohsen M, Bar-Shavit R, Catane R, Ekre HP. Modulation of neovascularization and metastasis by species of heparin. Adv Exp Med Biol 1992;313:317–27.
9. Takaoka M, Naomoto Y, Ohkawa T, et al. Heparanase expression correlates with invasion and poor prognosis in gastric cancers. Lab Invest 2003;83:613–22.
10. Gohji K, Hirano H, Okamoto M, et al. Expression of three extracellular matrix degradative enzymes in bladder cancer. Int J Cancer 2001;95:295–301.
11. Ginath S, Menczer J, Friedmann Y, et al. Expression of heparanase, Mdm2, and erbB2 in ovarian cancer. Int J Oncol 2001;18:1133–44.
12. Rohloff J, Zinke J, Schoppmeyer K, et al. Heparanase expression is a prognostic indicator for postoperative survival in pancreatic adenocarcinoma. Br J Cancer 2002;86:1270–5.
13. Sheng H, Shao J, Morrow JD, Beauchamp RD, DuBois RN. Modulation of apoptosis and Bcl-2 expression by prostaglandin E_2 in human colon cancer cells. Cancer Res 1998;58:362–6.
14. Tsujii M, Kawano S, Tsuji S, Sawaoka H, Hori M, DuBois RN. Cyclooxygenase regulates angiogenesis induced by colon cancer cells. Cell 1998;93:705–16.
15. Tsujii M, Kawano S, DuBois RN. Cyclooxygenase-2 expression in human colon cancer cells increases metastatic potential. Proc Natl Acad Sci U S A 1997; 94:3336–40.
16. Shattuck-Brandt RL, Lamps LW, Heppner Goss KJ, DuBois RN, Matrisian LM. Differential expression of matrilysin and cyclooxygenase-2 in intestinal and colorectal neoplasms. Mol Carcinog 1999;24: 177–87.
17. Kambayashi T, Alexander HR, Fong M, Strassmann G. Potential involvement of IL-10 in suppressing tumor-associated macrophages. Colon-26-derived prostaglandin E_2 inhibits TNF-α release via a mechanism involving IL-10. J Immunol 1995;154:3383–90.
18. Shamma A, Yamamoto H, Doki Y, et al. Up-regulation of cyclooxygenase-2 in squamous carcinogenesis of the esophagus. Clin Cancer Res 2000;6:1229–38.

19. Wilson KT, Fu S, Ramanujam KS, Meltzer SJ. Increased expression of inducible nitric oxide synthase and cyclooxygenase-2 in Barrett's esophagus and associated adenocarcinomas. Cancer Res 1998;58:2929–34.
20. Leahy KM, Koki AT, Masferrer JL. Role of cyclooxygenases in angiogenesis. Curr Med Chem 2000;7:1163–70.
21. Jones MK, Wang H, Peskar BM, et al. Inhibition of angiogenesis by nonsteroidal anti-inflammatory drugs: insight into mechanisms and implications for cancer growth and ulcer healing. Nat Med 1999;5:1418–23.
22. Rapraeger AC, Krufka A, Olwin BB. Requirement of heparan sulfate for bFGF-mediated fibroblast growth and myoblast differentiation. Science 1991;252:1705–8.
23. Elkin M, Ilan N, Ishai-Michaeli R, et al. Heparanase as mediator of angiogenesis: mode of action. FASEB J 2001;15:1661–3.
24. Yayon A, Klagsbrun M, Esko JD, Leder P, Ornitz DM. Cell surface, heparin-like molecules are required for binding of basic fibroblast growth factor to its high affinity receptor. Cell 1991;64:841–8.
25. Vlodavsky I, Friedmann Y. Molecular properties and involvement of heparanase in cancer metastasis and angiogenesis. J Clin Invest 2001;108:341–7.
26. Boring CC, Squires TS, Tong T, Montgomery S. Cancer statistics, 1994. CA Cancer J Clin 1994;44:7–26.
27. Sagar PM, Gauperaa T, Sue-Ling H, McMahon MJ, Johnston D. An audit of the treatment of cancer of the oesophagus. Gut 1994;35:941–5.
28. Daly JM, Fry WA, Little AG, et al. Esophageal cancer: results of an American College of Surgeons Patient Care Evaluation Study. J Am Coll Surg 2000;190:562–72; discussion 572–3.
29. Kimura M, Haisa M, Uetsuka H, et al. TNF combined with IFN-α accelerates NF-κB-mediated apoptosis through enhancement of Fas expression in colon cancer cells. Cell Death Differ 2003;10:718–28.
30. Toyoshima M, Nakajima M. Human heparanase. Purification, characterization, cloning, and expression. J Biol Chem 1999;274:24153–60.
31. El-Assal ON, Yamanoi A, Ono T, Kohno H, Nagasue N. The clinicopathological significance of heparanase and basic fibroblast growth factor expressions in hepatocellular carcinoma. Clin Cancer Res 2001;7:1299–305.
32. Okada Y, Yamada S, Toyoshima M, Dong J, Nakajima M, Sugahara K. Structural recognition by recombinant human heparanase that plays critical roles in tumor metastasis: hierarchical sulfate groups with differential effects and the essential target disulfated trisaccharide sequence. J Biol Chem 2002;277:42488–95.
33. Kutchera W, Jones DA, Matsunami N, et al. Prostaglandin H synthase 2 is expressed abnormally in human colon cancer: evidence for a transcriptional effect. Proc Natl Acad Sci U S A 1996;93:4816–20.
34. Mikami S, Ohashi K, Usui Y, et al. Loss of syndecan-1 and increased expression of heparanase in invasive esophageal carcinomas. Jpn J Cancer Res 2001;92:1062–73.
35. Ohkawa T, Naomoto Y, Takaoka M, et al. Localization of heparanase in esophageal cancer cells: respective roles in prognosis and differentiation. Lab Invest 2004;84:1289–304.
36. Inoue H, Nanayama T, Hara S, Yokoyama C, Tanabe T. The cyclic AMP response element plays an essential role in the expression of the human prostaglandin-endoperoxide synthase 2 gene in differentiated U937 monocytic cells. FEBS Lett 1994;350:51–4.
37. Inoue H, Yokoyama C, Hara S, Tone Y, Tanabe T. Transcriptional regulation of human prostaglandin-endoperoxide synthase-2 gene by lipopolysaccharide and phorbol ester in vascular endothelial cells. Involvement of both nuclear factor for interleukin-6 expression site and cAMP response element. J Biol Chem 1995;270:24965–71.
38. Shao J, Sheng H, Inoue H, Morrow JD, DuBois RN. Regulation of constitutive cyclooxygenase-2 expression in colon carcinoma cells. J Biol Chem 2000;275:33951–6.
39. Masunaga R, Kohno H, Dhar DK, et al. Cyclooxygenase-2 expression correlates with tumor neovascularization and prognosis in human colorectal carcinoma patients. Clin Cancer Res 2000;6:4064–8.
40. Friedmann Y, Vlodavsky I, Aingorn H, et al. Expression of heparanase in normal, dysplastic, and neoplastic human colonic mucosa and stroma. Evidence for its role in colonic tumorigenesis. Am J Pathol 2000;157:1167–75.
41. Masferrer JL, Leahy KM, Koki AT, et al. Antiangiogenic and antitumor activities of cyclooxygenase-2 inhibitors. Cancer Res 2000;60:1306–11.
42. Hanahan D, Folkman J. Patterns and emerging mechanisms of the angiogenic switch during tumorigenesis. Cell 1996;86:353–64.
43. Rahman MA, Dhar DK, Masunaga R, Yamanoi A, Kohno H, Nagasue N. Sulindac and exisulind exhibit a significant antiproliferative effect and induce apoptosis in human hepatocellular carcinoma cell lines. Cancer Res 2000;60:2085–9.
44. Form DM, Auerbach R. PGE_2 and angiogenesis. Proc Soc Exp Biol Med 1983;172:214–8.
45. Kelly T, Miao HQ, Yang Y, et al. High heparanase activity in multiple myeloma is associated with elevated microvessel density. Cancer Res 2003;63:8749–56.
46. Herschman HR. Prostaglandin synthase 2. Biochim Biophys Acta 1996;1299:125–40.
47. Oshima M, Dinchuk JE, Kargman SL, et al. Suppression of intestinal polyposis in ApcΔ716 knockout mice by inhibition of cyclooxygenase 2 (COX-2). Cell 1996;87:803–9.
48. Matsuura H, Sakaue M, Subbaramaiah K, et al. Regulation of cyclooxygenase-2 by interferon γ and transforming growth factor α in normal human epidermal keratinocytes and squamous carcinoma cells. Role of mitogen-activated protein kinases. J Biol Chem 1999;274:29138–48.
49. Tjian R, Maniatis T. Transcriptional activation: a complex puzzle with few easy pieces. Cell 1994;77:5–8.
50. LeClair KP, Blanar MA, Sharp PA. The p50 subunit of NF-κB associates with the NF-IL6 transcription factor. Proc Natl Acad Sci U S A 1992;89:8145–9.
51. Schubert SY, Ilan N, Shushy M, Ben-Izhak O, Vlodavsky I, Goldshmidt O. Human heparanase nuclear localization and enzymatic activity. Lab Invest 2004;84:535–44.